Received: 21 December 2021 | Revised: 27 January 2022 | Accepted: 10 February 2022

DOI: 10.1111/ffe.13680

ORIGINAL ARTICLE

FFEMS Fatigue & Fracture of Engineering Materials & Structures WILEY

Nonlinear fatigue life prediction model based on the theory of the S-N fatigue damage envelope

Fredrik Bjørheim | **Dimitrios G. Pavlou** | **Sudath C. Siriwardane**

Department of Mechanical and Structural Engineering and Materials Science, University of Stavanger, Stavanger, Norway

Correspondence
Fredrik Bjørheim, Department of Mechanical and Structural Engineering and Materials Science, University of Stavanger, Stavanger N-4036, Norway.
Email: fredrik.bjorheim@uis.no

Abstract

A nonlinear model is proposed in light of the theory of isodamage curves, to assess the cumulative fatigue damage under multistage loading. The isodamage curves were developed through the theory of the S-N fatigue damage envelope, proposed by Pavlou. The adopted functional form of the fatigue damage is a commonly accepted general form. In the present work, a stress function for the fatigue life exponent is derived with the aid of the S-N curve only. In the proposed nonlinear model, no adjusting parameters are necessary for fatigue damage estimation. The fatigue life prediction of the derived model is compared with experimental results of various alloys and existing models. The comparison is made for C35, C45, Al-2024-T42, 15HM, A336 GR 5, and A387 GR22 for two-stage loading high-low and low-high, and Al 6082-T6 for multistage loading.

KEYWORDS

fatigue damage envelope, fatigue life, isodamage, nonlinear damage model, variable amplitude loading

1 | INTRODUCTION

The commonly applied damage rule, first proposed by Palmgren[1] and popularized by Miner,[2] does not properly account for variable amplitude loading (VAL). The model is applied through a linear summation of the consumed life fraction per stress amplitude, where it is assumed that failure occurs when the summation reaches unity. However, the model is inherently flawed, due to its negligence regarding the perspective of loading sequence,[3] consequently resulting in failure commonly occurring at a sum lower than unity for decreasing load amplitude histories but higher than unity for their increasing amplitude counterparts.[4] This is due to the fact that the fatigue damage accumulation material mechanisms are nonlinear. In fact, if the applied stress amplitude were reduced from high to low fatigue loading, a crack might have initiated in the initial stress amplitudes, which would not have initiated for the equivalent percentage for the subsequent low amplitude fatigue loading.[5]

Despite the shortcomings of Miner's rule, it is still commonly recommended in both Eurocode[6] and DNVGL.[7] This is due to the perspective that an accumulation model is required to design for VAL, that it is

generally simple to follow, and that the formula yields acceptable life prediction for uniform random loading histories.[8–11] The inherent error or uncertainty in Miner's rule for decreasing load amplitude spectra could result in catastrophic consequences. However, it is commonly accounted for through the application of a Design Fatigue Factor, used in conjunction with a design S-N curve which already has a low probability of failure (2.3% in DNVGL),[12,13] resulting in a more conservative design due to the application of Miner's rule.

This highlights the need for further research within the field regarding damage accumulation, at which several attempts have been made both from the viewpoint of theoretical approaches or reflections regarding the S-N curve and regarding the measurement of fatigue damage.[14–24]

Examples of this might be such as the double linear damage rule (DLDR), developed by Manson et al.,[25–27] on the basis of the suggestion by Grover,[28] which shows good agreement with experimental results. The principle in Manson's work is to apply two linear damage rules, which were first categorized as crack initiation and propagation but later categorized as Phase I and Phase II. This arises from the perspective that no measurable cracks could be observed after the phase of initiation had been surpassed, whereas a difference between the phases was recognized.

Another example might be the isodamage lines. The theory of isodamage lines is based on the assumption that the S-N curve has a damage state of 100%, whereas the damage state for a given number of cycles and stress amplitudes falls on straight lines and can, therefore, be related to the next stress amplitude.

Subramanyan[29] proposed a set of straight isodamage lines which converge toward the knee point in an S-Log(N) diagram. Moreover, this model can then determine an equivalent n/N_f for the subsequent stress amplitude. The model implies that the number of cycles required to induce a certain level of damage increases with a reduction in stress amplitude and vice versa, thus being able to capture the loading sequence effect of high to low and low to high. An interesting paper which experimentally confirms the theory of isodamage lines for Al-2024-T42 is that by Pavlou,[30] in which isodamage curves were experimentally derived through the correlation of damage evolution with the evolution of surface hardness.

In contrast to Subramanyan, Hashin and Rotem proposed a set of isodamage lines which converge toward the intercept of the S-Log(N) curve with the stress axis.[31] The effectiveness of this model was criticized in Hectors and De Waele.[15] Most of the researchers have found that Subramanyan is the more favorable of the two theories. However, both models have been found to be slightly non-conservative.

Rege and Pavlou proposed a one-parameter nonlinear fatigue damage accumulation model, based on the concept of isodamage curves.[32] The objective was to reduce the non-conservatism of the model proposed by Subramanyan. It was successfully achieved for low to high two-stage loading, whereas, for high to low amplitude loading, little difference was observed.

Aeran et al. demonstrated the importance of a model which is based on the commonly available S-N curves.[33,34] This arose from the perspective that several damage models, depending on additional material parameters, had been proposed. This, in turn, resulted in the models not being readily applicable. Thus, they proposed a damage model based on the commonly applied S-N curves, in conjunction with a damage transfer concept to account for loading sequence. The damage model simply depends on the parameter N_f, commonly found in traditional S-N curves, whereas the transfer concept also depends on the related stress amplitudes.

Mesmacque et al. proposed a sequential law.[35] The sequential law does not depend on more than the full range of the S-N curve, which it is suggested can be found by the limited dataset of commonly used S-N curves through the Wöhler curve modeling proposed by Kohout and Vechet.[36] The model has, for instance, been adopted in research to estimate the remaining fatigue life of railway bridges.[37] However, even though the study showed a better estimation in comparison to the Miner's rule, a significant deviation from the real fatigue life was observed.

Presenting a function of evaluating the damage envelope and developing a simple tool for damage estimation and life prediction, which depends only on the readily available S-N curves, are the major objectives of this paper. The theory of the S-N fatigue damage envelope proposed by Pavlou[38] is adopted, and a generally accepted damage function formalism for damage evolution is utilized to develop the new damage model. The proposed model can be used for any metallic material, with any type of loading, and it depends only on the general S-N curve.

2 | THE CONCEPT OF THE FATIGUE DAMAGE ENVELOPE

The fatigue damage envelope proposed by Pavlou is based on the hypothesis that the area bounded by the stress and cycles' axes and the S-N curve provides a fatigue damage map for the material. However, in contrast to Subramanyan and Hashin and Rotem's common methodologies for isodamage lines, the proposed

isodamage curves in Pavlou's theory are not straight lines converging only at the knee point or at the ultimate stress S_u at the stress axis, as can be seen in Figure 1A,B, respectively. In fact, the isodamage curves proposed[38] are curved and converge at both the knee point and at the ultimate stress, as can be seen in Figure 2. The argument for the isodamage curve, in contrast to the isodamage straight line, originates from the fact that the S-N curve has a damage state of $D=1$, as in failure, whereas both the S and the N axes have a damage state of $D=0$. Consequently, it should be assumed that no damage is accumulated when the number of cycles is $n=0$, and the same follows for the scenario where the stress amplitude is equal (or beneath) the fatigue limit. It should be mentioned here that the stress-axis and the cycles-axis are the normalized quantities presented in Equations 1 and 2.

$$\sigma_i^* = \frac{\sigma_i - S_e}{S_u - S_e} \quad 0 \le \sigma_i^* \le 1 \tag{1}$$

$$n_i^* = \frac{n_i}{N_e} \quad 0 \le n_i^* \le 1 \tag{2}$$

where σ_i is the applied stress amplitude, S_e is the fatigue endurance limit, S_u is the ultimate stress and N_e is the fatigue capacity at the knee-point stress, resulting in the normalized parameters σ_i^* and n_i^* both having values in the range of 0 to 1. A schematical representation of the damage accumulation path under four-stage loading history is shown in Figure 3. In fact, it can be seen that, for a subsequent stress amplitude, an equivalent normalized number of cycles has to be found.

The development of the curves can be performed through a heat transfer analysis in a finite element software, described in detail in Pavlou's paper.[38]

3 | NONLINEAR FATIGUE DAMAGE FUNCTION

An increase in the number of loading cycles by dn/n causes an increase in damage dD/D. Taking this concept into account, a generally accepted formulation for damage function D is based on the solution of the following differential equation:

$$\frac{dD}{D} = q(\sigma, m)\frac{dn}{n} \tag{3}$$

where $q(\sigma, m)$ is a parameter affected by the stress amplitude σ and the material properties m.

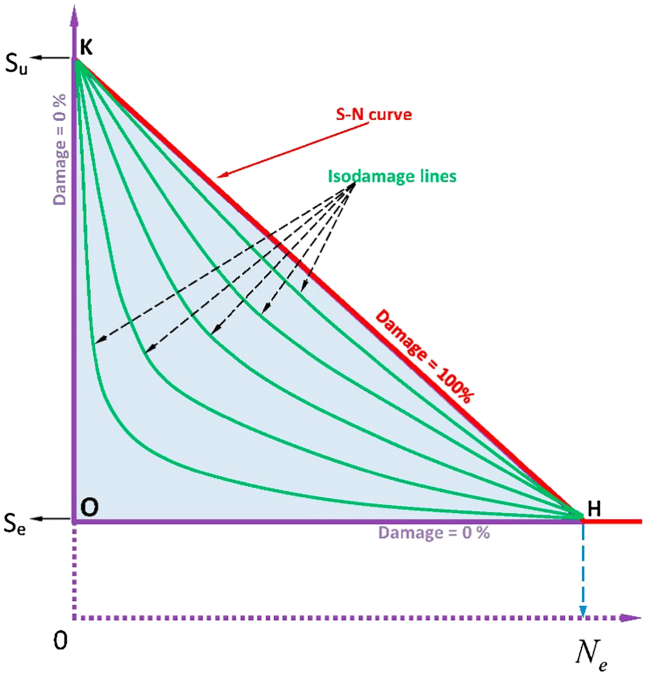

FIGURE 2 The isodamage lines within the S-N fatigue damage envelope. Reprinted from Pavlou[38] with permission from Elsevier, © 2018 [Colour figure can be viewed at wileyonlinelibrary.com]

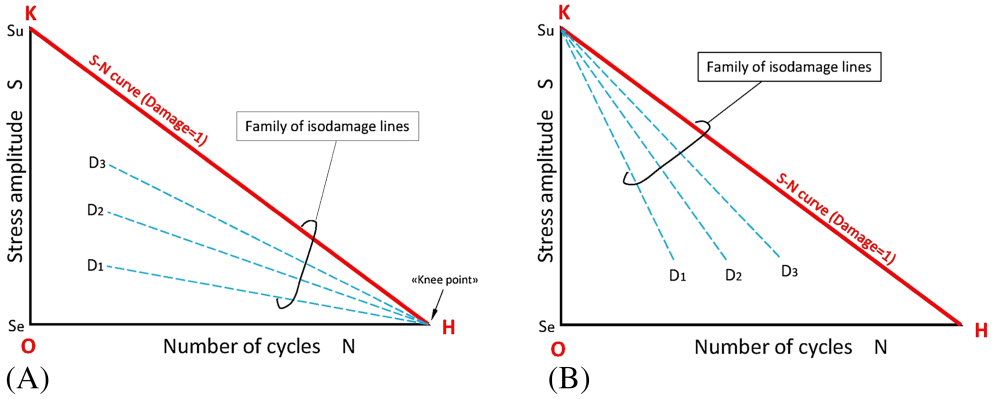

FIGURE 1 Isodamage lines converging: (A) at the knee point of the S-N curve, (B) at the S_u point. Reprinted from Pavlou[38] with permission from Elsevier, © 2018 [Colour figure can be viewed at wileyonlinelibrary.com]

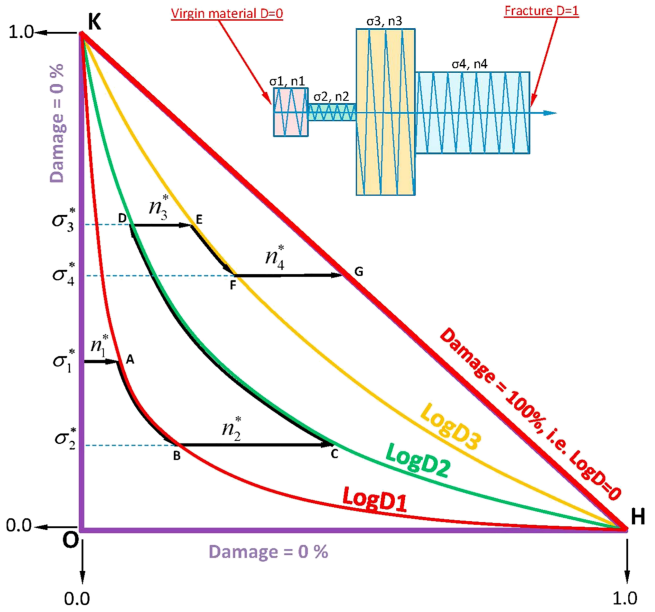

FIGURE 3 Schematical representation of the damage accumulation path under four-stage loading history. Reprinted from Pavlou[38] with permission from Elsevier, © 2018 [Colour figure can be viewed at wileyonlinelibrary.com]

The solution of Equation 3 yields

$$\mathrm{Log}(D) = q(\sigma, m)\mathrm{Log}(n) + C \tag{4}$$

where C is the integration parameter.

Taking into account the condition $D = 1$ for $n = N_f$, Equation 4 yields

$$C = -q(\sigma, m)Log(N_f) \tag{5}$$

With the aid of the above equation, Equation 4 can be written as follows:

$$\mathrm{Log}(D) = q(\sigma, m)\left(\mathrm{Log}(n) - Log(N_f)\right) \tag{6}$$

or

$$D = \left(\frac{n}{N_f}\right)^{q(\sigma,m)} \tag{7}$$

The exponent $q(\sigma, m)$ is accepted to be a function of the stress amplitude by all the existing research.[9,15,16,39] Both the final expression of the function $q(\sigma, m)$ and the number of material parameters m with their respective values depends upon the theoretical or experimental method which is adopted to develop a function, as there are both theoretical and experimental methods of defining damage. As the theoretical approach proposed by Pavlou[38] is adopted herein, the governing parameters for the resulting expression with its material parameters are related to the nature of the S-N curve. According to the theoretical background of the model, the S-N damage envelope[38] demonstrates the effect of the fatigue mechanisms, in damage accumulation in macroscopic level.

4 | DAMAGE ACCUMULATION UNDER MULTISTAGE LOADING

The nonlinear fatigue damage model in Equation 7 can be used to estimate the damage accumulation under multistage loading. For the sake of simplicity, Equation 7 will be initially applied to estimate the damage accumulation due to a two-stage loading history shown in Figure 4A.

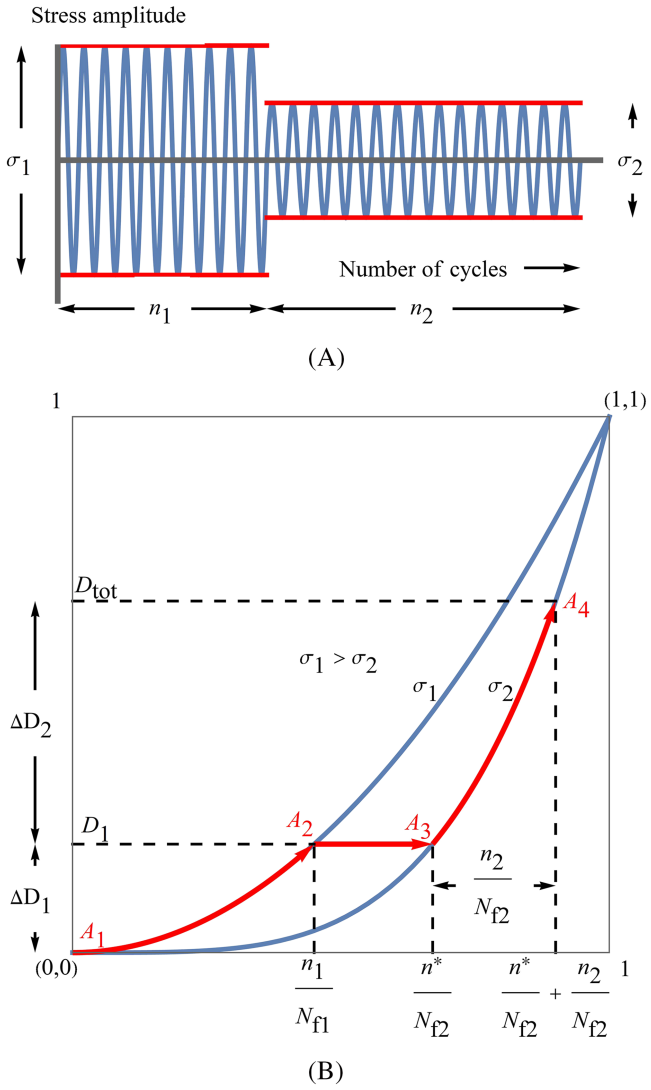

FIGURE 4 (A) Two-stage loading history and (B) damage accumulation path during two-stage loading history [Colour figure can be viewed at wileyonlinelibrary.com]

The damage accumulation during the first loading block (σ_1, n_1) is demonstrated by the path $A_1 \rightarrow A_2$ in Figure 4B. When the second loading block (σ_2, n_2) starts, damage D_1 has already been accumulated by the first loading block (σ_1, n_1). Therefore, the damage accumulation path for the second block (σ_2, n_2) starts from the point A_3 that corresponds to damage D_1. The damage accumulation path $A_3 \rightarrow A_4$ for the loading block (σ_2, n_2) lies on the isostress curve σ_2 and corresponds to the normalized number of cycles n_2/N_{f2} (see Figure 4B).

According to Equation 7, the total damage accumulation after the two loading blocks is

$$D_{tot} = \left(\frac{n^*}{N_{f2}} + \frac{n_2}{N_{f2}}\right)^{q(\sigma_2, m)} \tag{8}$$

The ratio n^*/N_{f2} corresponds to the starting point A_3 of the damage path $A_3 \rightarrow A_4$ of the second loading block (σ_2, n_2). Point A_3 corresponds to the same damage as the end point A_2 of the damage path $A_1 \rightarrow A_2$ of the first loading block (σ_1, n_1).

Therefore,

$$D_1 = \left(\frac{n_1}{N_{f1}}\right)^{q(\sigma_1, m)} \quad \text{for point } A_2 \tag{9}$$

and

$$D_1 = \left(\frac{n^*}{N_{f2}}\right)^{q(\sigma_2, m)} \quad \text{for point } A_3 \tag{10}$$

A combination of Equations 9 and 10 yields

$$\frac{n^*}{N_{f2}} = \left(\frac{n_1}{N_{f1}}\right)^{\frac{q(\sigma_1, m)}{q(\sigma_2, m)}} \tag{11}$$

With the aid of the above equation, Equation 8 yields

$$D_{tot} = \left(\left(\frac{n_1}{N_{f1}}\right)^{\frac{q(\sigma_1, m)}{q(\sigma_2, m)}} + \frac{n_2}{N_{f2}}\right)^{q(\sigma_2, m)} \tag{12}$$

The above equation can be generalized for multistage loading:

$$D_{tot} = \left(\left(\cdots\left(\left(\left(\frac{n_1}{N_{f1}}\right)^{\frac{q(\sigma_1, m)}{q(\sigma_2, m)}} + \frac{n_2}{N_{f2}}\right)^{\frac{q(\sigma_2, m)}{q(\sigma_3, m)}} + \frac{n_3}{N_{f3}}\right)^{\frac{q(\sigma_3, m)}{q(\sigma_4, m)}} + \cdots + \frac{n_{k-1}}{N_{f(k-1)}}\right)^{\frac{q(\sigma_{k-1}, m)}{q(\sigma_k, m)}} + \frac{n_k}{N_{f(k)}}\right)^{q(\sigma_k, m)} \tag{13}$$

According to the authors' knowledge, the existing nonlinear models in the literature commonly propose exponent ratios $q(\sigma_i, m)/q(\sigma_{i+1}, m)$ instead of exponent function $q(\sigma, m)$. The existing exponent ratios can be utilized only for the case that $D_{tot} = 1$, from which the following formulation can result:

$$\left(\cdots\left(\left(\left(\frac{n_1}{N_{f1}}\right)^{\frac{q(\sigma_1, m)}{q(\sigma_2, m)}} + \frac{n_2}{N_{f2}}\right)^{\frac{q(\sigma_2, m)}{q(\sigma_3, m)}} + \frac{n_3}{N_{f3}}\right)^{\frac{q(\sigma_3, m)}{q(\sigma_4, m)}} + \cdots + \frac{n_{k-1}}{N_{f(k-1)}}\right)^{\frac{q(\sigma_{k-1}, m)}{q(\sigma_k, m)}} + \frac{n_k}{N_{f(k)}} = 1 \tag{14}$$

Equation 14 is useful for estimating the remaining fatigue life $n_k/N_{f(k)}$ up to failure, but it is not capable of fatigue damage estimation or structural health monitoring for $D < 1$. Exponent $q(\sigma, m)$, instead of exponent's ratio $q(\sigma_i, m)/q(\sigma_{i+1}, m)$, has been proposed in Pavlou's phenomenological fatigue damage rule[30] and in the one-parameter fatigue model of Rege and Pavlou.[32] In the present work, an exponent function $q(\sigma, m)$ that does not contain any adjusting parameter is proposed for the first time. The new proposed function $q(\sigma, m)$ herein is based on the isodamage curves of the S-N fatigue damage envelope[38] and needs only the S-N curve of the material.

5 | QUANTIFICATION OF FATIGUE DAMAGE ENVELOPE RESULTS AND PROPOSED DAMAGE MODEL

The model is developed through quantification of the results found in a paper by Pavlou.[38] The selected S-N curve for analysis can be seen in Figure 5, which shows the simplified example of how damage mapping is performed. The variables of the axes are specified for the abscissa in Equation 1 and the ordinate in Equation 2.

The results provided by Pavlou included both the points and an equation to fit to the points, resulting in the following plot seen in Figure 6. For the sake of demonstration, an isostress line for $\sigma^* = 0.5$ can also be seen in the figure, in which each intersection between the damage curves and the isostress line determines a cycle ratio for each level of damage for the specific stress amplitude. Such an evaluation was performed from a normalized stress of 0.1 to 0.9 with a step size of 0.1. After the cycle ratios per damage level had been determined for the evaluated normalized stress levels, the damage curves were interpolated with the functional formalism as presented in Equation 7 to determine the stress dependent exponent. The resulting damage curves, where the ratio n/N_e has been normalized to n/N_f, can be seen in Figure 7.

The exponent in Equation 7 was then plotted as a function of normalized stress amplitude, with the objective of finding a relation with the normalized stress through curve interpolation, as can be seen in Figure 8. It was found that the best interpolation function was in the form as presented in Equation 15.

$$q(\sigma^*, m) = \frac{a}{\sigma^*} \tag{15}$$

where the parameter a was found to be $a = 6$, whereas σ^* is the normalized stress, as previously presented in Equation 1. Therefore,

$$q(\sigma, m) = \frac{a(S_u - S_e)}{(\sigma - S_e)} \tag{16}$$

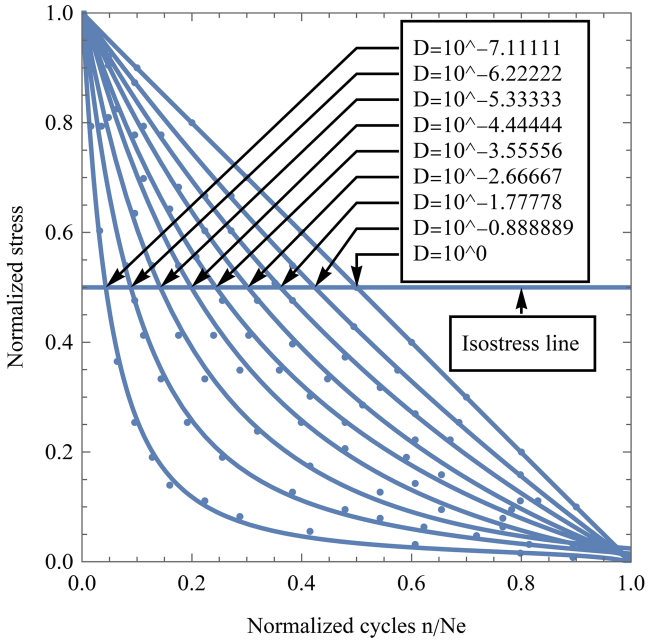

FIGURE 6 Method to develop the isostress damage curves [Colour figure can be viewed at wileyonlinelibrary.com]

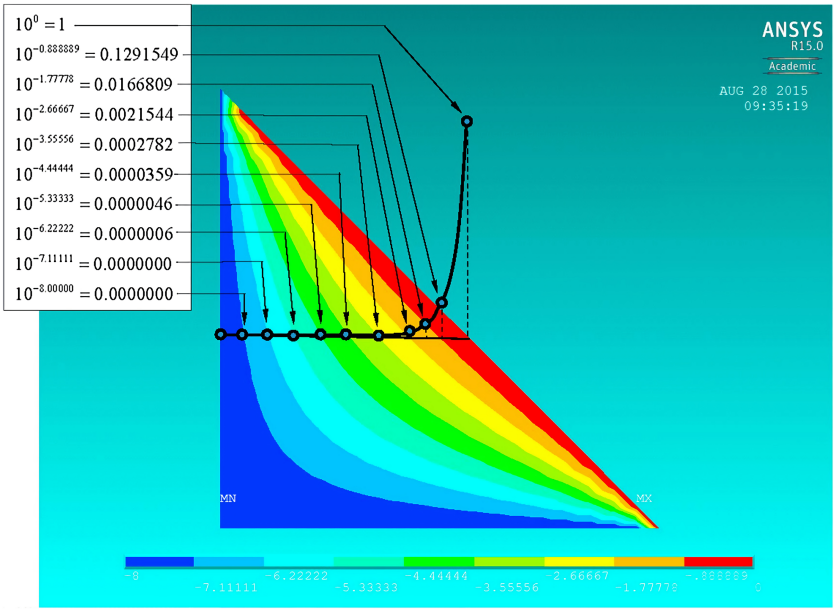

FIGURE 5 Isodamage curves including the damage value for each curve. Reprinted from Pavlou[38] with permission from Elsevier, © 2018 [Colour figure can be viewed at wileyonlinelibrary.com]

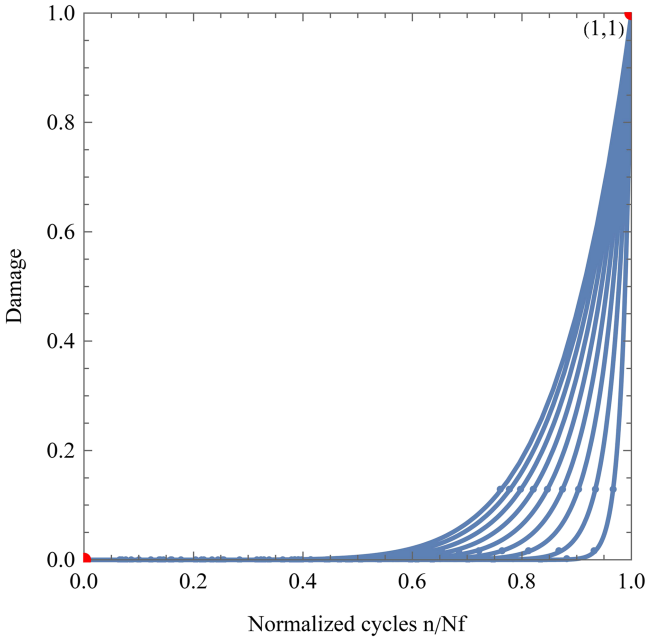

FIGURE 7 Isostress curves with the normalized quantity n/N_f [Colour figure can be viewed at wileyonlinelibrary.com]

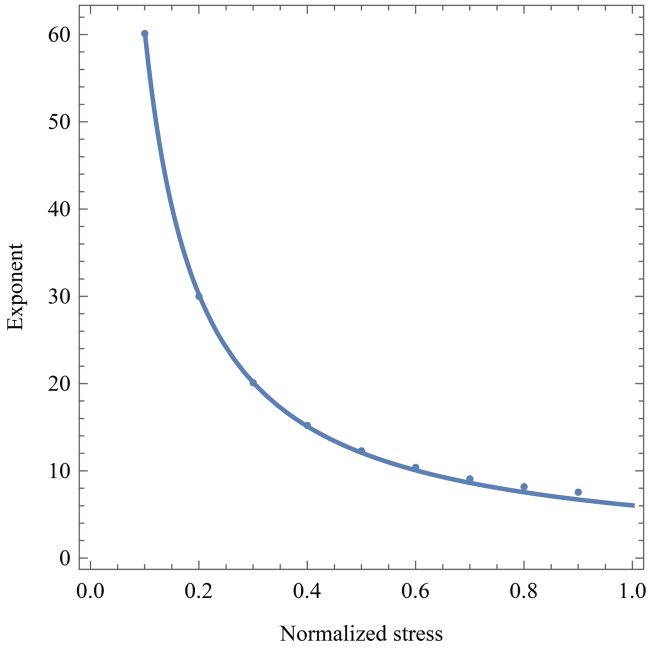

FIGURE 8 Damage exponent as a function of normalized stress amplitude [Colour figure can be viewed at wileyonlinelibrary.com]

inserting Equation 16 into Equation 7, the following nonlinear fatigue damage model can be obtained:

$$D = \left(\frac{n}{N_f}\right)^{\frac{a(S_u - S_e)}{\sigma_i - S_e}} \tag{17}$$

6 | IMPLEMENTATION AND VERIFICATION OF THE PROPOSED MODEL

The proposed model was verified and compared with other models for the following materials C45,[40] C35,[29] 15HM, A387 GR 22, A336 GR 5,[41] and Al-2024-T42[30] for two-stage loading, and Al 6082-T6[42] for multistage loading. The models adopted for the comparison are the Palmgren-Miner's rule,[1,2] Aeran,[33] Rege and Pavlou,[32] and Mesmacque.[35] Within the results used for verification, both two-stage loading and the results obtained for multistage loading were adopted. Therefore, it is practical to separate this section into two subsections regarding the two categories of results.

Throughout the verification and comparison section, the parameter "experimental remaining life" is the measured number of cycles in the last loading block before failure, whereas the parameter "calculated remaining life" is the estimated number of cycles in the last loading block before failure. For two-stage loading, the "experimental remaining life" is the measured number of cycles n_2 of the second block up to failure (Figure 4A) under the stress amplitude σ_2. The calculated remaining life is determined by Equation 12 for $D_{tot} = 1$, that is, $n_2 = N_{f2}\left(1 - \left(n_1/N_{f1}\right)^{q(\sigma_1,m)/q(\sigma_2,m)}\right)$. Further information regarding the loading histories can be found in the respective references.

6.1 | Verification and comparison of the model for two-stage loading

6.1.1 | C45 steel

C45 steel is a medium carbon steel, known to have a high wear resistance and good quenching and tempering capabilities. C45 steel is commonly applied for such items as bolts, fasteners, shafts, crankshafts, bigger gears, car parts and structures.[43–45] The material was in the normalized condition, and the cyclic loading was rotating bending, fully reversed stress-controlled two-stage loading. The mechanical properties of the material are as follows: yield strength $\sigma_y = 371.7$ MPa, ultimate tensile strength $S_u = 598.2$ MPa and the knee-point stress $S_e = 262.8$ MPa. The cyclic stress amplitudes applied were 331.5 MPa and 284.4 MPa, where both high-low and low-high loading were used, resulting in the high to low loading sequence being 331.5–284.4 MPa, whereas the low to high loading sequence was 284.4–331.5 MPa. The results obtained from the comparison for both the high-low and low-high loading sequences can be seen in Figure 9. The solid line

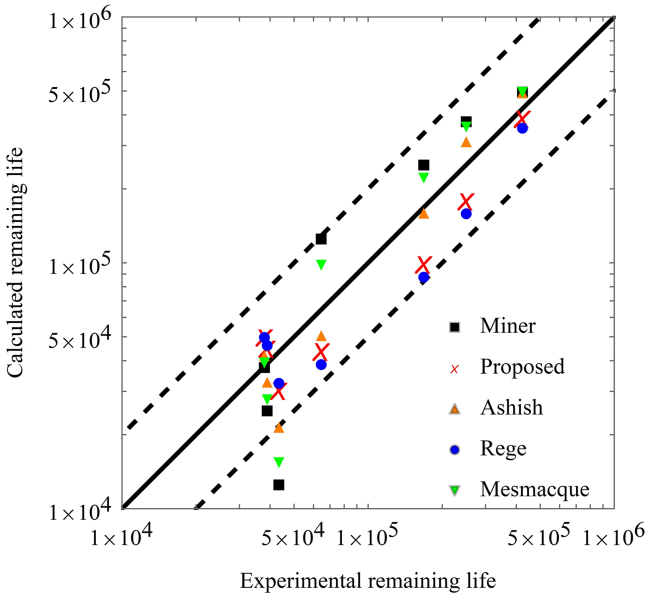

FIGURE 9 Comparison of calculated and experimental remaining life for C45 steel two-block loading [Colour figure can be viewed at wileyonlinelibrary.com]

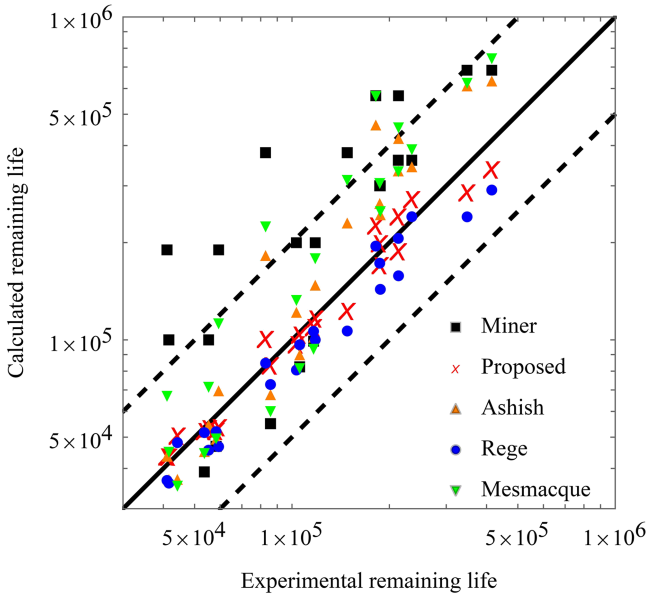

FIGURE 10 Comparison of calculated and experimental remaining life for C35 steel two-block loading [Colour figure can be viewed at wileyonlinelibrary.com]

refers to ideal conformity of the results, whereas the dotted lines represent a scatter band with a coefficient of two.

6.1.2 | C35 steel

C35 steel is also a medium carbon steel, with slightly less carbon (0.35%–0.39%) than the C45 steel, resulting in a reduction in hardness, although its application areas are within the same domain. The mechanical properties of the specimens are yield strength $\sigma_y = 324$ MPa, ultimate tensile strength $S_u = 458$ MPa and knee-point stress $S_e = 255$ MPa. The specimens were ground in the longitudinal direction, and no heat treatment was given. The tests were performed as two-stage block loading, under cantilever rotating beam fatigue, with stress-controlled conditions, at 3000 rpm = 50 Hz. Stress amplitudes of 373, 353, 334, 294, and 275 were used, in various combinations, for two-stage block loading for both high-low and low-high. The results obtained from the comparison for both the high-low and low-high loading can be seen in Figure 10. The solid line refers to ideal conformity of the results, whereas the dotted lines represent a scatter band with a coefficient of two.

6.1.3 | 15HM, A387 GR 22, and A336 GR 5

These different steels are commonly used in the electrical power and petroleum chemistry industries under high temperature and pressure. For such items as steam heater coils, plates for boiler drums and pressurized vessels, forgings and bars for boiler parts, pressurized vessels and turbines and pipelines of superheated steam, 15HM (13CrMo4-5) is commonly applied.[46–48] Meanwhile, A387 GR 22 (10CrMo9-10) is commonly used in seamless pipes for steam conditions reaching high temperatures, such as pressurized parts of boilers powered by fossil fuels and heat recovery system generators.[49,50] A336 GR 5 can also be found to be applicable in the same domain.[51] The specimens were all fatigued under stress controlled fully reversed ($R = -1$) tension compression loading, at 20 Hz in room temperature (21°C). Each type of material was tested under the two-stage block loading sequences of high-low and low-high. The stress amplitudes 375 MPa and 400Mpa were adopted for 15HM steel, 475 MPa and 525 MPa for A387 GR 22, and 375 and 425 MPa for A336 GR5. The results obtained from the comparison for both the high-low and low-high loading can be seen in Figure 11. The solid line refers to ideal conformity of the results, whereas the dotted lines represent a scatter band with a coefficient of two.

6.1.4 | Al-2024-T42

Al-2024-T42 is an aluminum-copper-magnesium-manganese, which is solution heat treated and naturally aged to a substantially stable condition. Al-2024 is

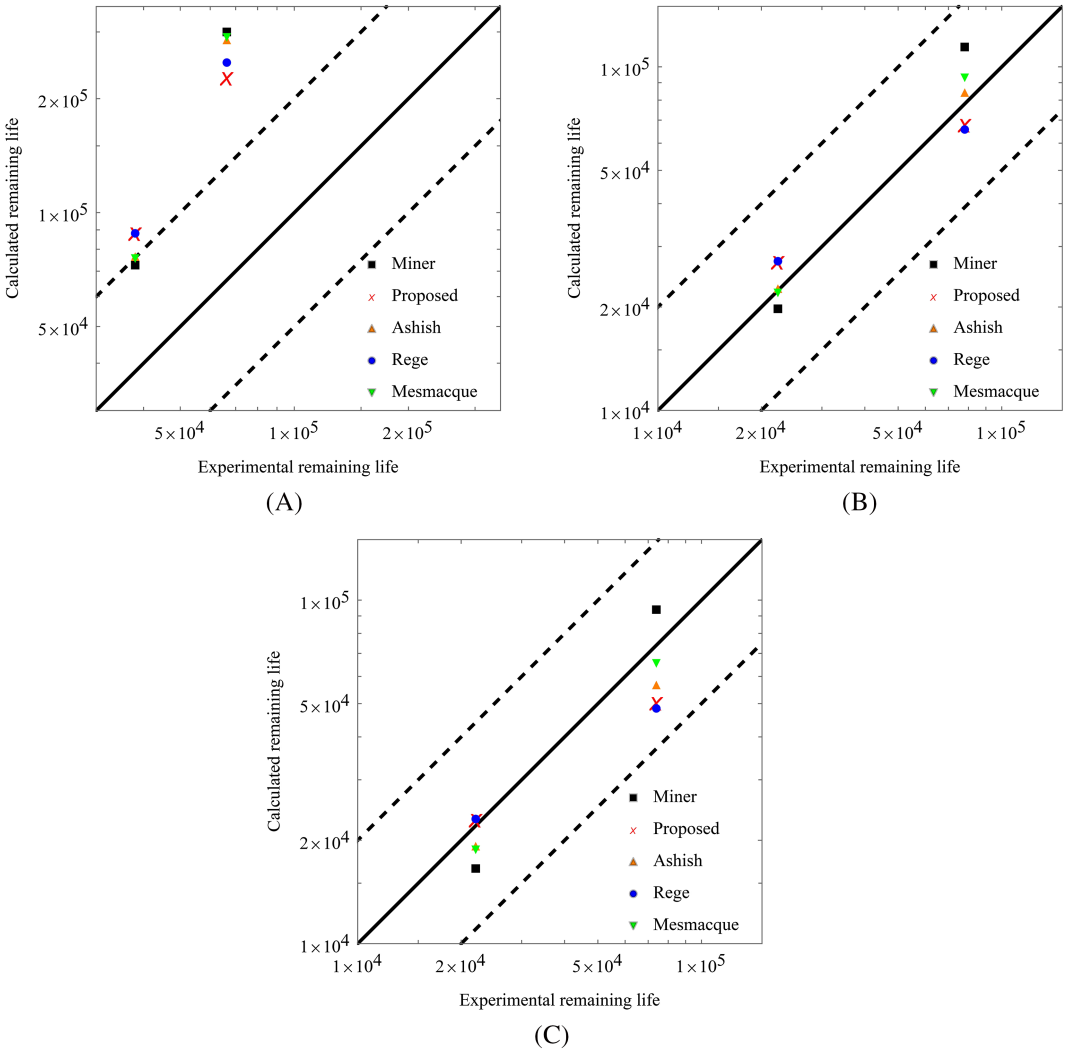

FIGURE 11 Comparison of calculated and experimental remaining life for (A) 15HM, (B) A387 GR22, and (C) A336GR5 subjected to two-block loading [Colour figure can be viewed at wileyonlinelibrary.com]

commonly used in such items as airframes, wing tension members, shear webs and ribs, due to the requirement for high strength to weight ratio in conjunction with good fatigue performance.[52–54] The Al-2024-T42 was fatigued under fully reversed ($R = -1$) uniaxial tension compression, with a frequency of 25 Hz at stress amplitudes of 150 and 200 MPa, from high to low and low to high, resulting in 150–200 and 200–150 MPa loading. However, it is well known that aluminum alloys do not exhibit a clear knee-point stress.[55,56] Therefore, it was decided to adopt a knee point of 0 MPa. The results obtained from the comparison for both the high-low and low-high loading can be seen in Figure 12. The solid line refers to ideal conformity of the results, whereas the dotted lines represent a scatter band with a coefficient of two.

6.2 | Verification and comparison of the model for multistage loading

6.2.1 | Al-6082-T6

Al-6082-T6 is a high-strength aluminum-magnesium-silicon alloy, which is solution heat treated and then artificially aged at a temperature of about 170–200°C.[54,57] The 6082 alloy has similar characteristics to those of the commonly used 6061 alloy. In the T6 condition, the alloy will also have slightly higher mechanical properties and will provide good machinability. Al-6082 is commonly adopted for such items as rods, bars, machining stock, structural profiles and seamless tubing.[58,59] The specimens were acquired as plates of 8 mm thickness, which were machined to dog bone specimens. Thereafter, the

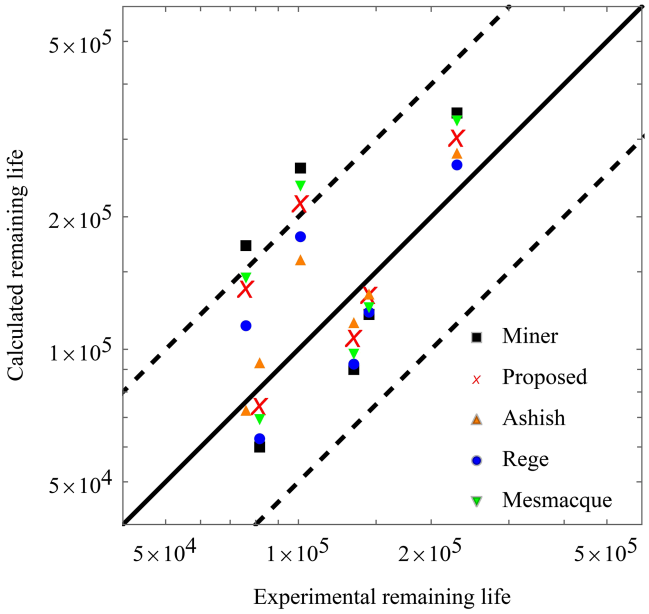

FIGURE 12 Comparison of calculated and experimental remaining life for Al-2024-T42 subjected to two-block loading [Colour figure can be viewed at wileyonlinelibrary.com]

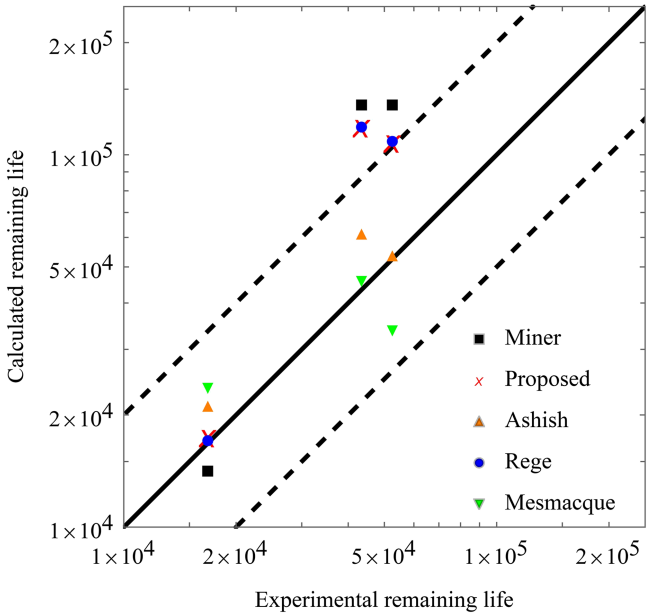

FIGURE 13 Comparison of calculated and experimental remaining life for Al-6082-T6 subjected to multilevel block loading [Colour figure can be viewed at wileyonlinelibrary.com]

specimens were subjected to uniaxial constant amplitude fatigue. The mechanical properties of the material are as follows: yield stress $\sigma_y = 347$ MPa, ultimate tensile stress $S_u = 370$ MPa, whereas the fatigue knee point S_e again is defined as 0, due to the common fatigue curve seen in aluminum alloys. The maximum stresses which were used in the various blocks are 240, 260, 280, and 305 MPa in the low-high and high-low staircase loading, with the addition of random loading in the sequence 280, 305, 260, and 240 MPa. The results obtained from the comparison for the three aforementioned scenarios can be seen in Figure 13. The solid line refers to ideal conformity of the results, whereas the dotted lines represent a scatter band with a coefficient of two.

7 | DISCUSSION

The proposed model is inherently simple to follow for practicing engineers, and both an estimation of the intermediate damage level and a prediction of remaining fatigue capacity can be performed. To carry out an analysis using the proposed model, the only requirement is the commonly used S-N or Wöhler curves, readily available in standards, which can, alternatively, be developed for the specific material or detail category if desired. From the results, it can be seen that the model generally obtains good to somewhat conservative results as regards the C35 and the C45 materials, which are ferritic pearlitic low-carbon steels. Furthermore, for the materials A387 Grade 22 and A336 GR 5, it was found that the model would provide good estimations, well within the scatter bands plotted with a coefficient of two. However, none of the models provided very good results for the 15 HM stainless steel. The results which deviate the most are those for the high to low loading, and the researcher who published the results stated that the specimen experienced early activation of Lüders bands,[41] resulting in a concentration of crystallographic defects, which accelerates the fatigue damage process. However, the results for the low to high loading are also non-conservative for the proposed and all compared models. For the material Al-2024-T42, with the assumption that the fatigue knee-point stress is set as zero, the model also has reasonable accuracy. However, for Al-6082-T6 with the same assumption, under multilevel block loading, the model has a result which is very accurate for a load increase test, whereas the load reduction (at the dashed line) and random loading (outside the dashed line) resulted in fairly non-conservative estimations. It should be highlighted that the proposed damage function herein is simply validated for cyclic loading with stepwise variable amplitude in order to check the effectiveness of the model to consider the material memory effect and to address the effect of the loading sequence in fatigue life prediction. The proposed function can also be implemented to random (irregular) service loading with the aid of a counting method (e.g., Rainflow method). However, even with the aid of a counting method,

direct implementation of the proposed model to irregular loading spectra yields numerical error accumulation in long loading histories. To this end, a multilinear damage summation technique for utilizing nonlinear models in spectrum loading and a new counting method has recently been proposed by Pavlou[9] and can be adopted by the proposed damage function.

In fact, it can also be considered to be a framework for how to develop fatigue damage accumulation formulas through the theory of the S-N fatigue damage envelope. This is from the perspective that, herein, a general, simplistic form of an S-N curve and a triangular envelope, as presented in Figure 5, was adopted, with a generally accepted formulation for damage, as presented in Equation 7, to develop a damage function. However, material specific, detail category specific or environmentally specific S-N curves might also be investigated, by applying the method explained herein in conjunction with the theory of the S-N fatigue damage envelope proposed by Pavlou.[38]

Furthermore, a short discussion regarding the theory of the S-N fatigue damage envelope is appropriate here. During the analysis of the isodamage curves proposed by Pavlou, it was found that, if the abscissa were transformed to the parameter n/N_f in contrast to n/N_e, but the ordinate was maintained as the normalized stress in accordance with Equation 1, the isodamage curves would be as presented in Figure 14. It can be seen that, within the domain of high amplitude low cycle fatigue, the Palmgren–Miner rule might be somewhat accurate,

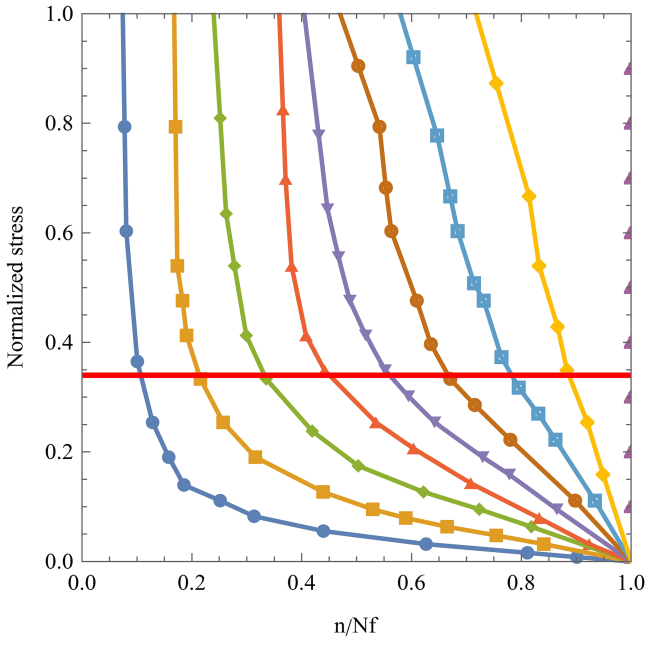

FIGURE 14 normalized isodamage curves [Colour figure can be viewed at wileyonlinelibrary.com]

whereas it will vastly deviate within the domain of low amplitude high cycle fatigue. This is from the perspective that, within the domain of high cycle fatigue, the majority of the fatigue life is spent in the initiation stage, whereas low cycle fatigue is dominated by crack propagation.[60,61] This means that, for the high-low fatigue loading transition, a crack might be initiated in the high amplitude loading, which could have taken nearly the entire fatigue capacity for the low amplitude fatigue loading. However, for the low-high transition, the low amplitude fatigue loading region might all have been spent on crack initiation, which would have occurred within the few first cycles within the high amplitude fatigue loading, thus resulting in the commonly accepted phenomenon of the linear damage rule, namely that the sum of the cycle ratios will be greater than unity for low-high loading but less than unity for high-low loading.[14] Furthermore, regarding the higher normalized stress amplitudes, Dowling specified that "the sequence effects do not occur if all of the levels cause significant plastic straining, which is consistent with the observation that the initiation period is short in the low cycle region."[62] In this regard, C35, for instance, can be considered, with material parameters of yield strength $\sigma_y = 324\,\text{MPa}$, ultimate tensile strength $S_u = 458\,\text{MPa}$ and knee-point stress $S_e = 255\,\text{MPa}$. The consequence is a cyclic stress amplitude equivalent to the yield strength of the material, resulting in a normalized stress of $\sigma^* = 0.34$. It can be seen from the figure that, if all stress amplitudes are higher than a normalized stress of 0.34, the relation between various stress amplitudes will, for the most part, behave linearly, where the deviation from the linear behavior will increase with n/N_f. Thus, it can be seen that the theory proposed by Pavlou clearly demonstrates the variable amplitude relation which has been documented by researchers.

For the derivation of the functional form of q in Equation 16, and the derived value of a in Equation 15, the usual engineering S-N curve which is demonstrated by a straight line passing the ultimate stress *Su* and the knee-point *Se* is used for the sake of simplicity. The corresponding triangular damage envelope in Figure 5[38] has been derived in terms of the normalized parameters of Equations 1 and 2. Therefore, the derivation of the damage map within the envelope of Figure 5 and the corresponding isodamage lines are universal. Since the derived function q in Equation 16 and the parameter a in Equation 15 are based on the isodamage lines of the universal triangular damage envelope, they include the material properties *Su*, *Se*, and *Ne* of any material and are universal too. Of course, Finite Element analysis can be performed for the specific S-N curve of each material and the function q considering the detailed nature of the S-N curve can be carried out. However, it seems that

Equation 16 is simple for engineering applications and provides sufficient accuracy in fatigue life prediction.

Almost all the known nonlinear rules are based on concepts of the rules of Manson-Halford,[27] Subramanyan,[29] Hashin-Rotem,[31] and so on. The majority of the existing damage accumulation rules provide only ratios of damage exponents $q(\sigma_i,m)/q(\sigma_{i+1},m)$, and they cannot propose the function $q(\sigma,m)$. Therefore, they can only predict the duration of the last loading block before failure $D=1$, but they cannot estimate the real-time accumulated damage at any stage ($D<1$) during loading. On the other hand, they are not valid for both HCF and LCF because some of the models (Figure 1) assume isodamage lines converging at the knee point of the S-N curve and they are valid only for large number of loading cycles (HCF), and other models assume isodamage lines converging at the *Su* point and they are valid for high stress amplitude (LCF). The proposed fatigue model has the following advantages versus the existing models: (a) It is based on nonlinear isodamage lines that take into account the damage map of the whole S-N damage envelope (Figure 2) and it is valid for all the fatigue stages, both HCF and LCF, and (b) it proposes a nonlinear exponent function $q(\sigma,m)$ instead of damage exponent ratios $q(\sigma_i,m)/q(\sigma_{i+1},m)$ and has the capability for estimation of the fatigue damage accumulation at any stage of the loading history.

8 | CONCLUSIONS

a. A new nonlinear fatigue damage accumulation model is proposed in light of the theory of the S-N fatigue damage envelope, proposed by Pavlou. Consequently, the expression is dependent on the readily available S-N curves only.
b. The resulting damage function was verified in experimental results and compared with other models for several materials, indicating good fatigue damage estimation.
c. A general framework for how to adopt the theory of the S-N curve to develop damage functions for general and case-specific S-N curves has been presented.
d. The theory of the S-N fatigue damage envelope has been discussed and compared in regard to commonly accepted relations within the fatigue damaging process.

ACKNOWLEDGEMENT

The authors are grateful for the financial support provided by the Norwegian Ministry of Education during this project. Furthermore, the group wishes to thank the publisher for allowing the reuse of figures.

AUTHOR CONTRIBUTIONS

Fredrik Bjørheim: Conceptualization, methodology, formal analysis, visualization, and writing-original draft. **Dimitrios G. Pavlou:** Conceptualization, methodology, formal analysis, writing-review and editing, and supervision. **Sudath C. Siriwardane:** Methodology, formal analysis, writing-review and editing, and supervision.

DATA AVAILABILITY STATEMENT

The data that support the findings of this study are available on request from the corresponding author. The data are not publicly available due to privacy or ethical restrictions.

REFERENCES

1. Die PA, von Kugellagern L. *Zeitschrift Des Vereines Deutscher Ingenieure*. 1924;58(14):339-341.
2. Miner MA. Cumulative damage in fatigue. *J Appl Mech*. 1945; 12(3):A159-A164.
3. Jang J, Khonsari MM. On the prediction of fatigue life subjected to variable loading sequence. *Fatigue Fract Eng Mater Struct*. 2021;44(11):2962-2974.
4. Peng Z, Huang H-Z, Zhu S-P, Gao H, Lv Z. A fatigue driving energy approach to high-cycle fatigue life estimation under variable amplitude loading. *Fatigue Fract Eng Mater Struct*. 2016; 39(2):180-193.
5. Li ZX, Ko JM, Chan THT. Modelling of load interaction and overload effect on fatigue damage of steel bridges. *Fatigue Fract Eng Mater Struct*. 2001;24(6):379-390.
6. Eurocode 3. Design of steel structures-Part 1–9: Fatigue, NS-EN 1993-1-9:2005+NA:2010
7. DNVGL, RP-C203: fatigue design of offshore steel structures, 2014
8. Carpinteri A, Vantadori S, Łagoda T, Karolczuk A, Kurek M, Ronchei C. Fatigue assessment of metallic components under uniaxial and multiaxial variable amplitude loading. *Fatigue Fract Eng Mater Struct*. 2018;41(6):1306-1317.
9. Pavlou D. A deterministic algorithm for nonlinear, fatigue-based structural health monitoring. *Comput Aided Civ Inf Eng*. 2021;1-23.
10. Singh A. The nature of initiation and propagation S-N curves at and below the fatigue limit. *Fatigue Fract Eng Mater Struct*. 2002;25(1):79-89.
11. He L, Akebono H, Sugeta A, Hayashi Y. Cumulative fatigue damage of stress below the fatigue limit in weldment steel under block loading. *Fatigue Fract Eng Mater Struct*. 2020; 43(7):1419-1432.
12. Lotsberg I. *Fatigue design of marine structures*. New York NY: Cambridge University Press; 2016.
13. Ciavarella M, D'antuono P, Papangelo A. On the connection between Palmgren-Miner rule and crack propagation laws. *Fatigue Fract Eng Mater Struct*. 2018;41(7):1469-1475.
14. Fatemi A, Yang L. Cumulative fatigue damage and life prediction theories: a survey of the state of the art for homogeneous materials. *Int J Fatigue*. 1998;20(1):9-34.
15. Hectors K, De Waele W. Cumulative damage and life prediction models for high-cycle fatigue of metals: a review. *Metals*. 2021;11(2):204-235.

16. Santecchia E, Hamouda AMS, Musharavati F, et al. A review on fatigue life prediction methods for metals. *Adv Mater Sci Eng*. 2016;2016:9573524.
17. Bjørheim F, Siriwardane SC, Pavlou D. A review of fatigue damage detection and measurement techniques. *Int J Fatigue*. 2022;154:106556.
18. Xia F-L, Zhu S-P, Liao D, Dantas R, Correia JAFO, De Jesus AMP. Isodamage curve-based fatigue damage accumulation model considering the exhaustion of static toughness. *Eng Fail Anal*. 2020;115:104575.
19. Zhu S-P, Hao Y-Z, de Oliveira Correia JAF, Lesiuk G, de Jesus AMP. Nonlinear fatigue damage accumulation and life prediction of metals: a comparative study. *Fatigue Fract Eng Mater Struct*. 2019;42(6):1271-1282.
20. Meneghetti G, Ricotta M, Atzori B. A synthesis of the push-pull fatigue behaviour of plain and notched stainless steel specimens by using the specific heat loss. *Fatigue Fract Eng Mater Struct*. 2013;36(12):1306-1322.
21. Zhu SP, Lei Q, Wang QY. Mean stress and ratcheting corrections in fatigue life prediction of metals. *Fatigue Fract Eng Mater Struct*. 2017;40(9):1343-1354.
22. Sun B, Yang L, Guo Y. A high-cycle fatigue accumulation model based on electrical resistance for structural steels. *Fatigue Fract Eng Mater Struct*. 2007;30(11):1052-1062.
23. Gao K, Liu G. Nonlinear time-varying fatigue reliability analysis based on the improved toughness exhaustion model. *Fatigue Fract Eng Mater Struct*. 2021;44(12):3482-3498.
24. Teng Z, Wu H, Boller C, Starke P. Thermodynamic entropy as a marker of high-cycle fatigue damage accumulation: example for normalized SAE 1045 steel. *Fatigue Fract Eng Mater Struct*. 2020;43:2854-2866.
25. Manson SS, Nachtigall AJ, Ensign CR, Freche JC. Further investigation of a relation for cumulative fatigue damage in bending. *J Eng Ind*. 1965;87(1):25-35.
26. Manson SS. Interfaces between fatigue, creep, and fracture. *Int J Fract Mech*. 1966;2(1):327-363.
27. Manson SS, Halford GR. Practical implementation of the double linear damage rule and damage curve approach for treating cumulative fatigue damage. *Int J Fract*. 1981;17(2):169-192.
28. Grover HJ. An observation concerning the cycle ratio in cumulative damage. In: Subcommittee V, ed. *West Conshohocken*. PA: ASTM International; 1960:120-124.
29. Subramanyan S. A Cumulative Damage Rule Based on the Knee Point of the S-N Curve. *J Eng Mater Technol*. 1976;98(4):316-321. doi:10.1115/1.3443383
30. Pavlou DG. A phenomenological fatigue damage accumulation rule based on hardness increasing, for the 2024-T42 aluminum. *Eng Struct*. 2002;24(11):1363-1368.
31. Hashin Z, Rotem A. A cumulative damage theory of fatigue failure. *Mater Sci Eng A*. 1978;34(2):147-160.
32. Rege K, Pavlou DG. A one-parameter nonlinear fatigue damage accumulation model. *Int J Fatigue*. 2017;98:234-246.
33. Aeran A, Siriwardane SC, Mikkelsen O, Langen I. A new nonlinear fatigue damage model based only on S-N curve parameters. *Int J Fatigue*. 2017;103:327-341.
34. Aeran A, Siriwardane SC, Mikkelsen O, Langen I. An accurate fatigue damage model for welded joints subjected to variable amplitude loading. *IOP Conf Ser: Mater Sci Eng*. 2017;276:012038.
35. Mesmacque G, Garcia S, Amrouche A, Rubio-Gonzalez C. Sequential law in multiaxial fatigue, a new damage indicator. *Int J Fatigue*. 2005;27(4):461-467.
36. Kohout J, Věchet S. A new function for fatigue curves characterization and its multiple merits. *Int J Fatigue*. 2001;23(2):175-183.
37. Siriwardane S, Ohga M, Dissanayake R, Taniwaki K. Application of new damage indicator-based sequential law for remaining fatigue life estimation of railway bridges. *J Constr Steel Res*. 2008;64(2):228-237.
38. Pavlou DG. The theory of the S-N fatigue damage envelope: generalization of linear, double-linear, and non-linear fatigue damage models. *Int J Fatigue*. 2018;110:204-214.
39. Pavlou DG. Loading sequence effects on fatigue damage accumulation of offshore structures: a deterministic approach. In: *Paper presented at: Proceedings of the International Conference on Offshore Mechanics and Arctic Engineering - OMAE2017*.
40. Shang D-G, Yao W-X. A nonlinear damage cumulative model for uniaxial fatigue. *Int J Fatigue*. 1999;21(2):187-194.
41. Socha G. Prediction of the fatigue life on the basis of damage progress rate curves. *Int J Fatigue*. 2004;26(4):339-347.
42. Aid A, Amrouche A, Bouiadjra BB, Benguediab M, Mesmacque G. Fatigue life prediction under variable loading based on a new damage model. *Mater Des*. 2011;32(1):183-191.
43. Satish GJ, Madhusudhana HK, Nishant BH, Kottureshettar BB. Optimising cutting parameters in boring operation for C45 steel. *IOP Conf Ser: Mater Sci Eng*. 2020;872:012080.
44. Faur AS, Popa MS, Sattel S. Aproaches upon the influence of a new tap drill geometry on C45 steel processing. *Acta Techn Napocens Ser: Appl Math Mech Eng*, [S.l.], v. 59, n. 4, dec. 2016:393-398. ISSN 2393–2988. Available at: https://atna-mam.utcluj.ro/index.php/Acta/article/view/809
45. Selvam MD, Senthil P. Investigation on the effect of turning operation on surface roughness of hardened C45 carbon steel. *Austr J Mech Eng*. 2016;14(2):131-137.
46. Pietryka I, Golański G, Jasak J, Słania J, Urbańczyk P, Wieczorek P. Degradation of microstructure and mechanical properties of 15HM steel after 420,000 hours of service. *Adv Mater Sci Eng*. 2014;14(4):5-11.
47. Jackiewicz D, Kachniarz M, Rożniatowski K, et al. Temperature resistance of magnetoelastic characteristics of 13CrMo4-5 constructional steel. *Acta Phys Polon A*. 2015;127:614-616.
48. Gwoździk M. Characterization of oxide layers formed on 13CrMo4-5 steel operated for a long time at an elevated temperature. *Arch Metall Mater*. 2015;60:1783-1788.
49. Westin EM, Schnitzer R, Ciccomascolo F, Maderthoner A, Grönlund K, Runnsjö G. Austenitic stainless steel bismuth-free flux-cored wires for high-temperature applications. *Weld World*. 2016;60(6):1147-1158.
50. Hattingh DG, van Zyl C. Temperature distribution for a friction taper stud weld in thick wall 10CrMo910 steel. *R&D Journal*. 2012;28:37-45.
51. Dietrich L, Socha G. Accumulation of damage in A336 GR5 structural steel subject to complex stress loading. *Strain*. 2012;48(4):279-285.
52. Jefferson TB, Woods G, James FLAWF. *Metals and How to Weld Them*. 2nded. James F. Lincoln Arc Welding Foundation: Cleveland, Ohio; 1962.

53. Alcoa. Alloy 2024 sheet and plate—excellent fatigue properties-consistent performance. Accessed May 26, 2021. https://web.archive.org/web/20060827072154/http://www.alcoa.com/mill_products/catalog/pdf/alloy2024techsheet.pdf
54. Hatch JE. *Aluminum: Properties and Physical Metallurgy*. 1sted. Materials Park: Materials Park: ASM International; 1984.
55. Kaleva O, Orelma H, Petukhov D. Parameter estimation of a high-cycle fatigue model combining the Ottosen-Stenström-Ristinmaa approach and Lemaitre-Chaboche damage rule. *Int J Fatigue*. 2021;147:106153.
56. Brighenti R, Carpinteri A. A notch multiaxial-fatigue approach based on damage mechanics. *Int J Fatigue*. 2012;39:122-133.
57. Ericsson M, Sandström R. Influence of welding speed on the fatigue of friction stir welds, and comparison with MIG and TIG. *Int J Fatigue*. 2003;25(12):1379-1387.
58. Moreira PMGP, de Jesus AMP, Ribeiro AS, de Castro PMST. Fatigue crack growth in friction stir welds of 6082-T6 and 6061-T6 aluminium alloys: a comparison. *Theor Appl Fract Mech*. 2008;50(2):81-91.
59. Hydro. Alloy 6082. https://www.hydro.com/Document/Index?name=Alloy%206082.pdf&id=560720. Accessed 27.05, 2021.
60. Murakami Y, Miller KJ. What is fatigue damage? a view point from the observation of low cycle fatigue process. *Int J Fatigue*. 2005;27(8):991-1005.
61. Chowdhury P, Sehitoglu H. Mechanisms of fatigue crack growth—a critical digest of theoretical developments. *Fatigue Fract Eng Mater Struct*. 2016;39(6):652-674.
62. Dowling NE. Fatigue failure predictions for complicated stress-strain histories. T. & A.M. Report no. 337. Department of theoretical and applied mechanics university of Illinois; 1971.

How to cite this article: Bjørheim F, Pavlou DG, Siriwardane SC. Nonlinear fatigue life prediction model based on the theory of the S-N fatigue damage envelope. *Fatigue Fract Eng Mater Struct*. 2022;45(5):1480-1493. doi:10.1111/ffe.13680